Eddy-driven heterogeneity in sea ice during the ice-growth season

Josué Martínez-Moreno[1], Camille Lique[1], Claude Talandier[1]

[1]Laboratoire d'Océanographie Physique et Spatiale (LOPS), University of Brest/IFREMER/IRD/CNRS, Brest, France

Key Points:

- Mesoscale ocean eddies imprint heterogeneity on the sea-ice thickness during the freezing season.
- Eddies induce heterogeneity in the sea-ice thickness by locally changing the heat and salt fluxes at the ice-ocean interface.
- An increase in the eddy field intensity leads to an increase in the sea ice heterogeneity.

Corresponding author: Josué Martínez-Moreno, `josue.martinezmoreno@univ-brest.fr`

Abstract

Mesoscale eddies, generated by lateral gradients in salinity and temperature in the Arctic marginal ice zone (MIZ), are known to modulate the melting of sea ice in this region. Yet, it remains unclear if eddies also modify sea ice growth during the freezing season. Here, we use a set of idealized simulations to explore the sea ice growth above an eddying ocean. In the presence of eddies, mixing of the surface temperature and salinity fields induce heterogeneity in the heat and salt fluxes at the ice-ocean interface, ultimately imprinting heterogeneity on the sea ice thickness. A stronger eddy field imprints more heterogeneity in the sea ice thickness. More heterogeneity in the sea ice pack would likely impact the current and future evolution of the sea ice conditions in the Arctic, where a rapid transition towards an open-ocean regime is ongoing.

Plain Language Summary

Lateral variations of salinity and temperature in the Arctic Ocean caused by the melting or freezing of ice can result in ocean eddies (vortex-like features up to $\sim$ 100km in size). Previous studies have focused on how these eddies affect sea ice melting. However, it is not clear if eddies also play a role when the ice forms. Here, we use numerical simulations to see how these eddies influence the growth of sea ice. Eddies affect the temperature and salinity distributions at the ocean surface, which, in turn, modulate the thickness of sea ice as it forms. This eddy effect in the sea ice is important because it could impact the transitional zone between the open ocean and ice covered Arctic. Understanding these eddy-sea ice interactions is crucial to better understand the current and future states of the Arctic sea ice as it transitions to an summer ice free ocean.

1 Introduction

The Arctic sea ice thickness varies on a large variety of spatial and temporal scales ranging from a few meters to hundreds of kilometers and from days to several years (Lewis & Richter-Menge, 1998; Mcnutt & Overland, 2003), making sea ice fundamentally heterogeneous (Webster et al., 2022). On one hand, the variability at large-scale ($\mathcal{O} > 100$km) in sea ice thickness is driven by the atmospheric forcing and large-scale ocean dynamics (Mcnutt & Overland, 2003; Morison et al., 2006; Halloran et al., 2020). On the other hand, the spatial and temporal variations at small scales ($\mathcal{O} < 100$km) are dictated by atmospheric synoptic processes (Aue et al., 2022), lateral heat transport by eddies between the open ocean and ice-covered areas, and local sea ice advection by eddies (Cassianides et al., 2021; Gupta et al., 2020; Horvat & Tziperman, 2018). However, the source of spatial variability arising from oceanic small-scale processes (i.e. eddies) during the sea ice freezing season is yet to be fully characterized.

Eddies have been observed across the Arctic Ocean since the 1980s (Johannessen et al., 1987; Manley & Hunkins, 1985). Eddies are particularly prominent in the marginal ice zone (MIZ), the regions of transition between ice-free and ice-cover conditions characterized by sea ice concentrations between 15 and 80% (Kozlov et al., 2020). This is because the MIZ is also characterized by large lateral temperature and salinity gradients at the ocean surface, which fuel the generation of instabilities resulting in the formation of eddies (Brenner et al., 2020; Manucharyan & Thompson, 2017; Lu et al., 2015). Eddies in the Arctic range from a few hundred meters to tens of kilometres (submesoscale - mesoscale ranges). They can have a significant influence on the local mechanical and thermodynamical behaviour of sea ice, particularly in the MIZ (Manucharyan & Thompson, 2022), where they can locally modulate heat transport and vertical flux under sea ice, and thus the sea ice melt rates (Appen et al., 2018; Cassianides et al., 2023). Since there is a limited amount of in situ observations of the eddies under sea ice, many studies have used idealized simulations to better understand sea ice-eddy interactions. Some of these studies have shown the critical role eddies play in the melting of ice through the entrainment of warm subsurface waters into the mixed layer, enhanced Ekman-induced vertical motion of warm waters to the surface, and lateral mixing and advection of warm waters below sea ice (Gupta et al., 2020; Horvat & Tziperman, 2018; Manucharyan & Thompson, 2017). While these studies have focused on the effect ocean eddies have on sea ice melting, here we focus on the role eddies have in sea ice growth over the freezing season and their capacity to generate sea ice heterogeneity, specifically the spatial variability of the sea ice thickness.

In the present study, we use a hindcast performed with a very high-resolution model and a set of idealized simulations with different eddy fields forced with an idealized seasonal cycle to investigate the response of the ice thickness to the presence of eddies in the MIZ at the time of sea ice formation and over the freezing season.

2 Methods

The present study uses the output from two configurations: (i) "SEDNA" (Sea ice-EDdy resolving ocean paN-Arctic), a state-of-the-art pan-Arctic ocean-sea ice model (Talandier & Lique, 2023) and (ii) an idealized channel configuration. Both configurations are based on NEMO (Madec et al., 2022), coupled with a sea ice model (SI3; NEMO Sea Ice Working Group, 2022). SEDNA has a 1/60° horizontal resolution (which corresponds to $\sim$ 800m in the Arctic Basin) and 150 vertical levels. SEDNA starts from rest with an initial state based on the World Ocean Atlas 2009 (Locarnini et al., 2010) and is forced hourly with the ERA5 atmospheric reanalysis (Hersbach et al., 2020) over 2009–2015. We only look at the last year of the simulation (2014) to allow for an initial spinup. The setup used for the idealized simulations consists of a zonally reentrant channel that spans 1000 km zonally, 500 km meridionally, and 800 m in depth. The horizontal resolution is 2 km and the vertical has 100 levels with variable spacing that increases from 0.5 m at the surface to 18 m at the bottom. This resolution was chosen to resolve mesoscale features arising from baroclinic instabilities prescribed in the initial conditions. To limit the length scales of the flow, a logarithmic bottom drag is implemented. We use an f-plane approximation at around 80°N, a scale-aware velocity dependent bi-harmonic isopycnal tracer diffusivity, and a bi-harmonic horizontal viscosity. The vertical mixing is based on the turbulent kinetic energy closure from Blanke & Delécluse, 1993. The idealized simulations are forced by a daily climatology built from ERA5 over the period 1979 to 2021 of shortwave radiation, longwave radiation, and air temperature over the Arctic (north of 80°N). This forcing is spatially constant, and it does not include wind forcing. Forcing seasonally allows the retreat and formation of sea ice during summer and winter, respectively. The fluxes between the ice-ocean-atmosphere are computed using the NCAR bulk formula (Large & Yeager, 2009).

We perform a set of three spin-down experiments based on the idealized channel configuration to better understand the dependence of the ice on the presence and intensity of an eddy field. The first simulation (referred to as "no front") is initialized with horizontally uniform temperature and salinity fields. The vertical profile defined with a hyperbolic tangent, resembles a characteristic winter profile of the Arctic, where salinity dominates the stratification (β-ocean; Carmack, 2007), with a halocline separating the fresher and colder mixed layer from the saltier and warmer water below (Fig. S1a). The structure of the initial conditions for all the simulations is shown in Figure S1. The weak and strong front experiments are initialized with the same vertical profile as the no front experiment, but the temperature and salinity are redistributed meridionally to create a frontal structure that extends down to 75 m depth. This tracer redistribution preserves the same initial mean temperature and salinity across the different simulations. The intensity of the front was chosen to match typical sea surface temperature (SST) and salinity (SSS) differences between the ice covered region and the open ocean in the

MIZ ($\sim$ 1.3°C and $\sim$ 1 psu) found in the Arctic MIZ. The "strong front" experiment is initialized with this front, where cold and fresh water covers the northern half of the domain (Fig. S1c). The "weak front" experiment is analogous to the strong front, but the intensity of the front is scaled by a factor of 0.5 (0.65°C and 0.49 psu; Fig. S1b).

All the idealized simulations are initialized on May 1st with a sea ice thickness of 1 m over the entire model domain. The temperature and salinity fields include noise in the top 75 m to seed baroclinic instability. The idealized simulations are run for two years and the analyses presented hereafter comprise the freezing season of the second year of the simulation between September and December. The simulated length scales during the second year are proportional to the Rossby radius which is $\approx$ 10 km in all three simulations. These Rossby deformation radii are comparable to those found in the Arctic Ocean (Nurser & Bacon, 2014), and are fully resolved by the model resolution.

3 Heterogeneity of sea ice in a mesoscale resolving realistic model

Satellite images and high-resolution models have revealed abundant signatures of oceanic eddies in the Arctic sea ice (Cassianides et al., 2021; Kozlov et al., 2020; Manucharyan & Thompson, 2017). One example of this is visible in the sea ice thickness of October 2014 (at the beginning of the freezing season) from SEDNA. The spatial structure of sea ice is characterized by numerous eddies and filaments of different scales characteristic of oceanic eddies (Fig. 1a). Such features are up to 100 kilometres wide and persist for several days (Fig. 1d). SSS (Fig. 1b) and SST (Fig. 1c) show a similar rich mesoscale and submesoscale eddy field near the sea ice edge. Furthermore, the sea ice edge and sea ice thickness resemble the eddying structures observed in both the SSS and SST. In order for the sea-ice to reproduce these patterns, it is necessary that the sea ice is advected and/or formed within these structures. Additionally, these spatial patterns can be further modified by a combination of atmospheric and oceanic processes during the sea ice freezing period. For example, spatially variable radiative and freshwater fluxes will seed heterogeneity in the SST and SSS. This heterogeneity can then be mixed and stirred by eddies, increasing the spatial heterogeneity at the ocean surface. Once the surface reaches the freezing point and ice is formed, sea ice can then be advected by winds and ocean currents. All these processes are captured by the high-resolution hindcast shown in Fig. 1 and likely contribute to the sea ice thickness heterogeneity captured by the model. However, due to the complexity and entangled nature of these processes, quantifying their individual contributions remains challenging. Our approach to understand the specific role of eddies on the sea ice formation is to isolate the processes due to eddies, in a simplified dynamical system, without spatial variability in the atmospheric forcing nor wind forcing. Note that this idealized configuration resolves similar oceanic scales and features as those captured by the high-resolution model (Fig. 2 and S1), and allows us to focus on the impact eddies have on the heterogeneity of sea ice.

4 The role of eddies in the generation of sea ice heterogeneity

As in SEDNA, the idealized simulations *with eddies* (weak front and strong front) show a spatially heterogeneous sea ice thickness from September 20th onwards (Fig 2). Here again, the newly formed sea ice resembles the eddying features at the ocean surface. On the 15th of September, the no front experiment shows a homogeneous temperature field approximately 1°C above the freezing point. At the same date, the other experiments (weak and strong fronts) show a pronounced SST meridional gradient, where the northern part of the domain is close to the freezing point and the southern part is around 1.5°C warmer than the freezing point. As time progresses (successive rows of Fig. 2), the SST in the no front experiment reaches the freezing point in a couple of days and a homogeneous layer of ice forms, covering the full domain in one day (Fig. 2a). In contrast, the weak and strong front experiments show an SST and ice thickness rich in ed-

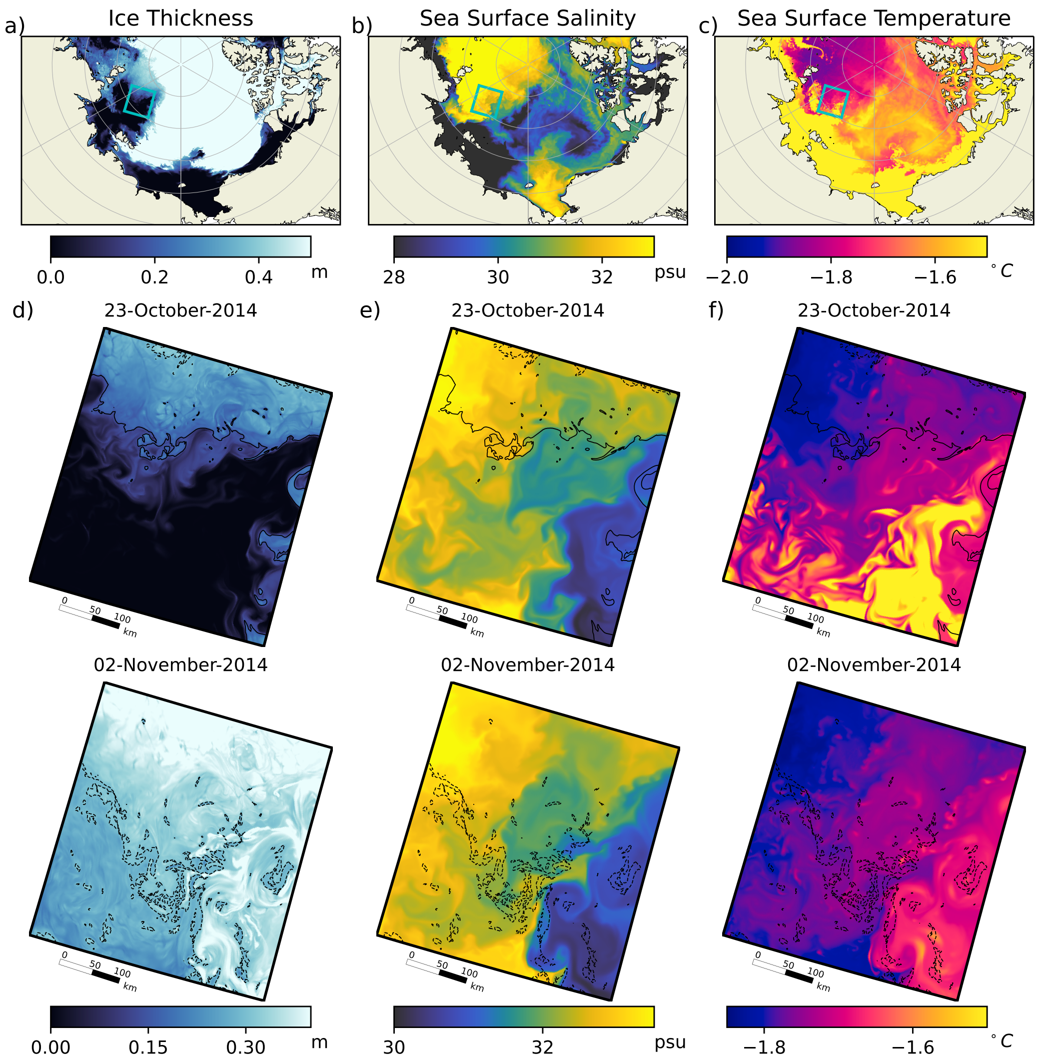

Figure 1. Snapshot of a) sea ice thickness (m), b) sea surface salinity (psu), and c) sea surface temperature (°C) on October 23, 2014 from SEDNA. Panels d, e, and f show two snapshots of the same quantities zoomed in the cyan box in panels a-c for October 23 2014 and November 2 2014. In panels d, e, and f the solid line contour shows the 15% ice concentration and the dashed line the 80% ice concentration.

dying features. In those, sea ice takes up to 14 days to fully cover the domain, since sea ice forms earlier or later over the colder and warmer SST regions, respectively (Fig. 2b, c, e, and f). Over time, sea ice thickness resembles these eddying features in the regions where the ocean surface has reached the freezing point. In other words, the presence of eddies makes the formation of ice spatially variable and the spatial length scale of the newly formed sea ice resembles the ocean mesoscale length scale.

The forcing of our idealized simulations does not include winds, nor any spatial heterogeneity in the atmospheric temperature and radiative fluxes. As such, sea ice heterogeneity can only be driven by heterogeneity arising during its formation or by eddy advection. At the initial stage, it arises necessarily from the heterogeneity in the ocean temperature and freezing point. The spatial variability of SSS and SST, quantified as their spatial standard deviation, describes where and when new ice will grow and the potential heterogeneity imprinted by the ocean state into the sea ice. The distributions of ice thickness, SST, and SSS are shown in Figure 3 for each experiment for the same dates as in Figure 2. Between September 15th and September 25th, the mean distributions of ice thickness, SST and SSS for the no front experiment show a narrow spread and a negligible standard deviation of 3×10^{-3} m in ice thickness, 7×10^{-3}°C in SST, and 5×10^{-3} psu in SSS. In other words, there is a homogeneous response of the ice thickness and ocean surface properties. During the ice growth period, sea ice in the no front simulation behaves as a slab of ice, and an increase in sea ice thickness results in a spatially constant SSS increase due to a homogeneous brine rejection across the domain. The weak front experiment has a wider distribution of SST and SSS compared to the no front experiment over the same period. The larger spread is a consequence of the advection and mixing of tracers by eddies, since eddies are well known to displace fluid parcels across large distances and enhance mixing of tracers (Montgomery, 1940). This signature lasts for several days until all the available heat is extracted from the mixed layer and the SST reaches the local freezing point. Synchronously, the SSS distribution shifts towards saltier values as sea ice forms and brine is rejected. The weak front experiment exhibits a larger mean standard deviation than the no front one (0.02 m in ice thickness, 0.02°C in SST, and 0.3 psu in SSS; Fig. 3). Finally, the experiment with a strong front has the widest distribution and the largest mean standard deviation in ice thickness (0.03 m), SST (0.03°C), and SSS (0.4 psu). Overall, the different experiments reveal that the heterogeneity of ice thickness is larger in the presence of a stronger eddy field.

In November and December, several months after the domain is fully covered by ice, the spatial variability in SST, SSS, and ice thickness retains a larger standard deviation in the presence of eddies in the weak and strong front experiments (Fig. 3; bottom rows). The strong front is still the experiment with the largest spatial variability and the initial heterogeneity imprinted at the beginning of the season is retained over the winter season. The presence of heterogeneity in the SST and SSS induces heterogeneity in the heat and salt fluxes at the ocean-ice interface. This is examined in the following section.

5 The role of the ocean-ice flux in setting up ice heterogeneity

At the beginning of the freezing season, the spatially heterogeneous ocean surface experiences cooling and thus regions where the SST is at the freezing point will use the additional heat flux lost to the atmosphere to grow ice. This is followed by brine rejection that increases the salt flux at the ice-ocean interface. After sea ice has started to form, an increase in SSS lowers the local freezing point and creates a feedback loop of cooling and brine rejection. This ice-ocean feedback in the presence of eddies produces a spatially variable freezing point under sea ice that makes spatially variable the heat and salt fluxes at the ocean surface throughout the freezing season.

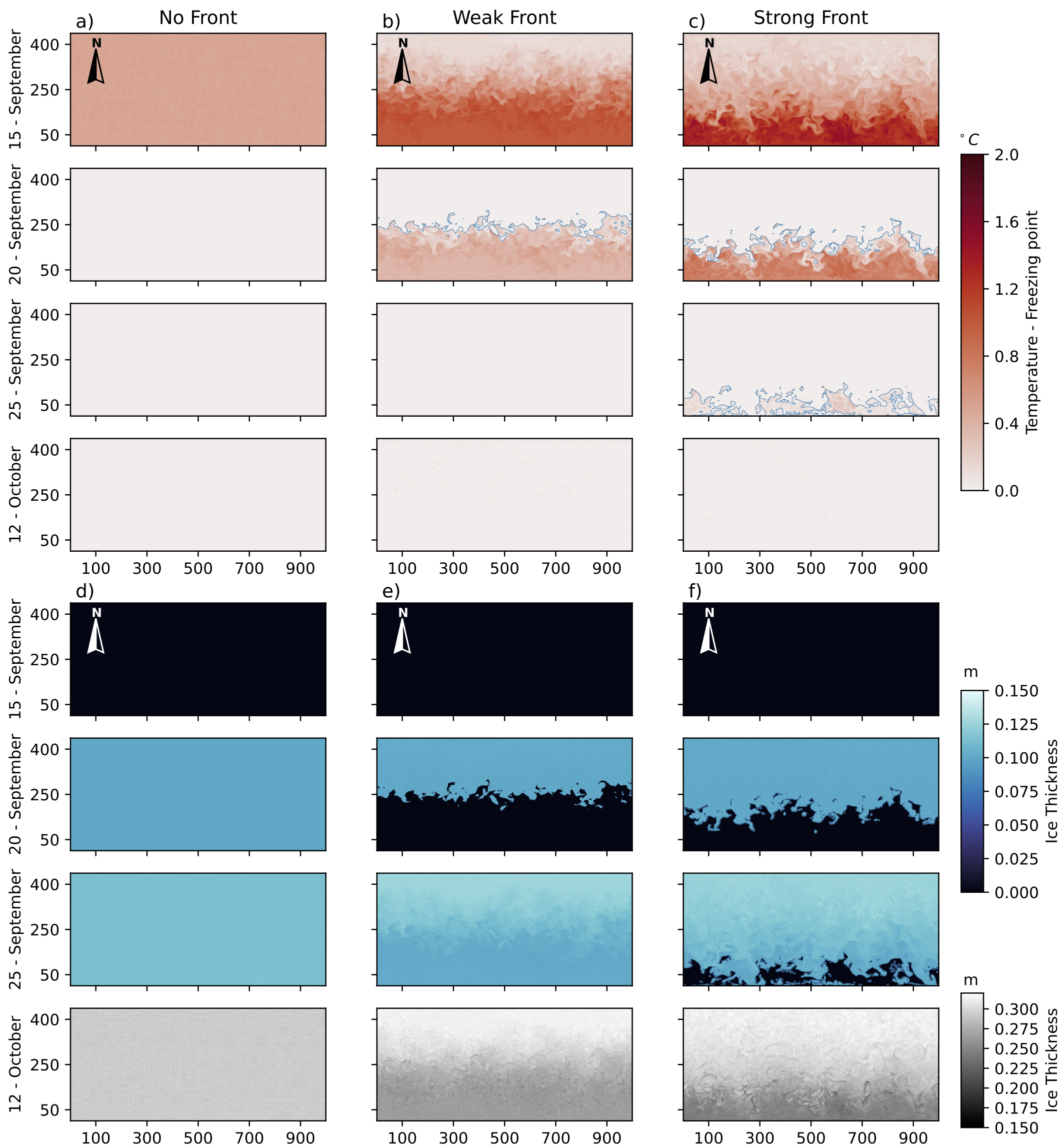

Figure 2. Sea surface temperature deviation from the local freezing point (a,b, and c, in °C) and ice thickness (d,e, and f, in m) for the three idealized experiments. The different rows show snapshots of the second-year simulation on the 15th of September, 20th of September, 25th of September, and 12th of October. The time evolution of the no front simulation is shown in columns a and d, the weak front in columns b and e, and the strong front in columns c and f. The blue lines in columns a, b, and c indicate the 0% ice concentration contour and the north of the domain is indicated with the compass.

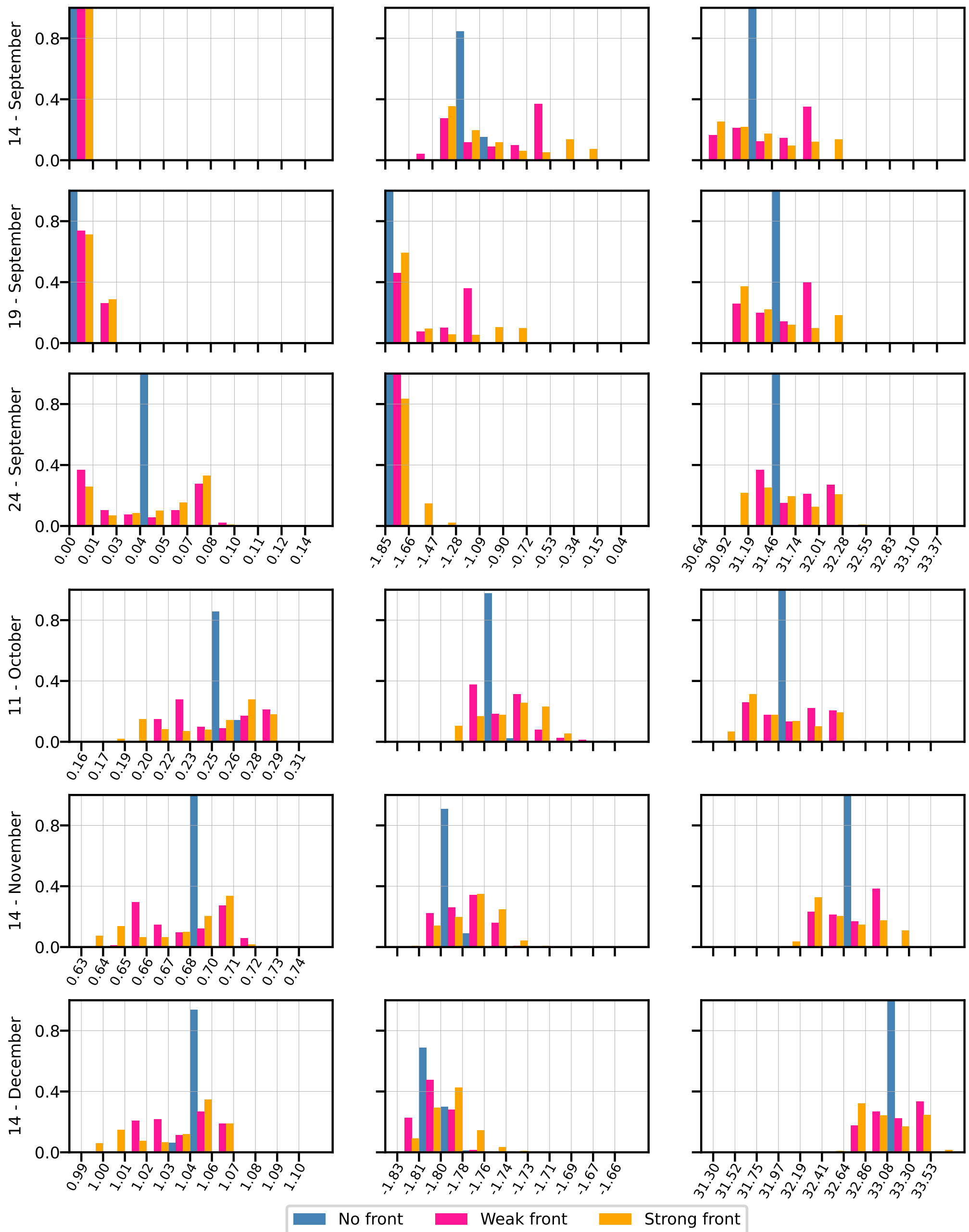

Figure 3. Normalized distribution over the domain of (a) ice thickness (m), (b) sea surface temperature (°C), and (c) sea surface salinity (psu) on the 15th of September, 20th of September, 25th of September, 12th of October, 15th of November, and 15th of December. Each colour corresponds to a different simulation: no front (blue), weak front (magenta), and strong front (orange). The different rows correspond to different dates of the simulations. Note the changes of x-axis between the different panels.

The heat and salt fluxes at the ice-ocean interface depend on the mechanisms of sea ice growth: basal growth, new ice formation in open ocean, and snow ice formation. Since the experiments exclude snow processes, the only fluxes during the freezing period are the open water formation and basal growth. The open water heat and salt fluxes (Fig. 4c and d) are different from zero when the ocean surface is in direct contact with the atmosphere and near the freezing point, at the beginning of the freezing season (15th of September). Figure 4c and d shows that the salt and heat fluxes in open water are only important during a short period ($\sim$ 1 month in October). Moreover, the spatial variability of these fluxes (shading in Fig. 4) increases with the intensity of the front. For example, the mean spatial standard deviation of the open water salt flux over the open-water ice-growth period (15th of September - 15th of October) is $5.37\times10^{-8}kg\ m^{-2}s^{-1}$ for the no front experiment, $22.06\times10^{-8}kg\ m^{-2}s^{-1}$ for the weak front experiment, and $26.75\times10^{-8}kg\ m^{-2}s^{-1}$ for the strong front experiment (Figure 4a). Analogous to the open water salt flux, the variance of the open water heat fluxes at the beginning of the freezing season is highly dependent on the ocean state. Overall, the no front experiment has the weakest spatial variations in both the salt and heat fluxes since the full domain responds at the same time, however, some important oscillations in the heat flux are visible. They are a numerical artifact, consequence of the model forming ice as a step-like function (Fig. 4d). The spatial heterogeneity in the salt and heat fluxes links the heterogeneity of an eddying ocean state to the ice thickness and accounts for all the feedbacks with the atmosphere (e.g. variable albedo and solar penetration).

Once the domain is partially or fully ice-covered, the largest fluxes at the ocean-sea ice interface correspond to basal growth. In our configuration, the transition between sea ice growth in open water to basal growth occurs at the end of October, and the basal growth fluxes reach a maximum in November after the full domain is covered by ice. Similar to the open water fluxes, the standard deviation of the heat and salt flux from ice bottom growth shows a larger spatial standard deviation in October in the presence of eddies (Fig. 4e and f). After November, the standard deviations of the basal growth salt and heat fluxes decrease and converge in all experiments, to $\sim -1.5\times10^{-6}kg\ m^{-2}s^{-1}$ and $-23Wm^{-2}$, respectively. This behavior reveals that the fluxes become more homogeneous as the sea ice conditions become thicker and more concentrated, since in all the simulations, surface eddies are strongly dissipated by the presence of sea ice during winter. Furthermore, the ice formation reaches a stable growth rate due to the spatially constant atmospheric forcing. The interplay between the fluxes from the open water and basal growth imprints the heterogeneity in the ice during the freezing season, emphasizing the critical role of ocean variability at the ice-ocean interface.

6 Discussion and Conclusions

The set of spin-down experiments, with varying intensities of the eddy field, shows an increase in the heterogeneity of sea ice depending on the intensity of the eddy field. Without eddies, ice formation is very fast, whilst, in the presence of eddies the ice formation starts a few days earlier, but it is slower lasting up to 14 days. Eddies are known to laterally transport heat and salt (Bashmachnikov et al., 2023; Fine et al., 2018). Thus, mixing of sea surface temperature and sea surface salinity by eddies, in addition to the ocean-atmosphere feedbacks responsible for determining the amount of ocean heat loss during the freezing season and the freezing point temperature, results in heterogeneous fluxes at the ocean surface. Therefore, eddies are able to imprint heterogeneity in the sea ice thickness during the freezing season. Although ice thickness is more spatially heterogeneous in the presence of eddies, there is only a negligible difference of the total sea ice volume between the simulations, because the climatological atmospheric forcing (same in all the experiments) is the main forcing determining the sea ice volume at the end of the season. This is despite a shallower mixed layer, a weaker stratification, and a warmer

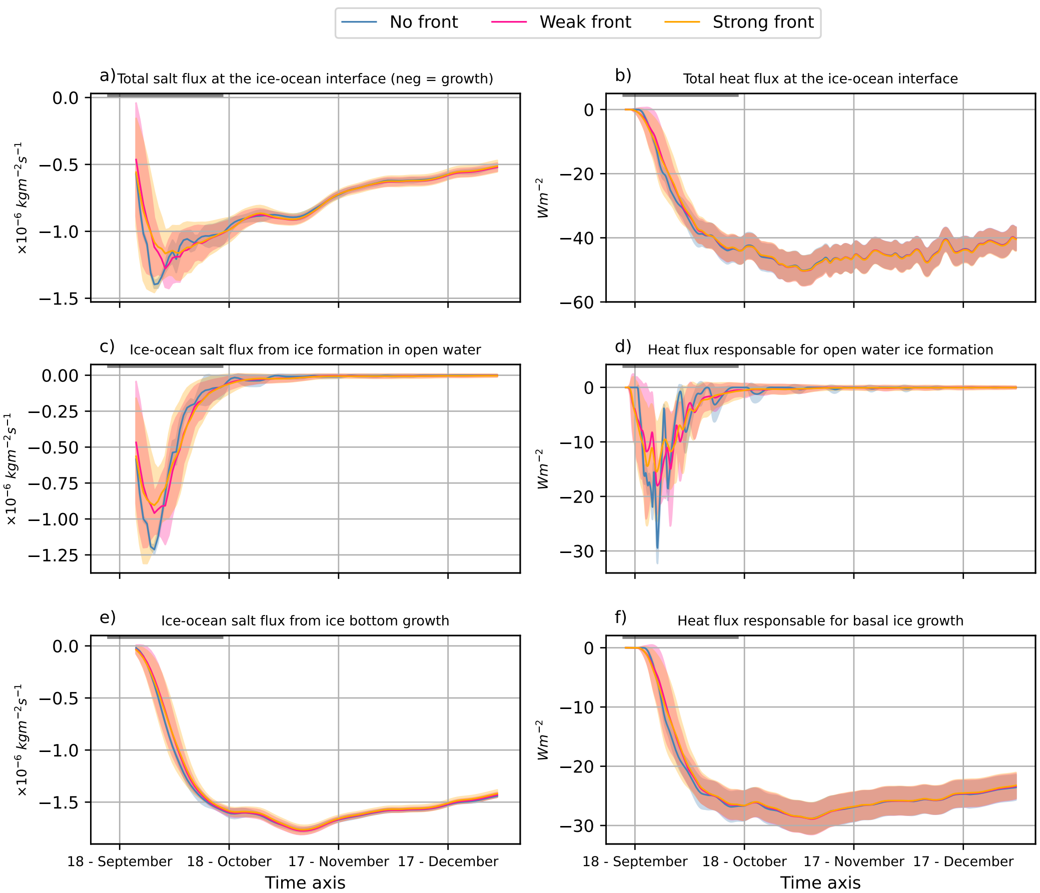

Figure 4. Salt and heat flux and their major components at the ocean surface for the three experiments: no front (blue), weak front (magenta), and strong front (orange). a) Total ice-ocean salt flux. b) Total heat flux at the ice-ocean interface. c) Ice-ocean salt flux in open water, which only includes the fluxes where new ice grows in open water areas. d) Heat flux used for open water ice formation. e) Ice-ocean salt flux from ice growth at the bottom. f) Heat flux used for bottom ice growth. Negative salt fluxes correspond to salinification and ice growth, while positive values are associated with freshening and ice melt. Negative heat fluxes correspond to cooling of the ocean surface, while positive values are associated with warming of the ocean surface. The shaded areas correspond to the spatial variance of each variable. The over-line between the 15th of September until the 15th of October indicates the open-water ice-growth period.

subsurface layer below the mixed layer due to enhanced mixing in the presence of eddies (not shown).

Our idealized simulations provide evidence that the ice can retain a memory of the ocean heterogeneity for several months after the time of formation. In fact, the heterogeneity of sea ice in snapshots during the melting season of the following year still retains some of this initial heterogeneity (not shown). The persistence of heterogeneity with similar length scales to oceanic eddies over the freezing season can be hypothesized to make the ice more brittle and prone to deform under atmospheric stress. It is interesting to note that the sea ice deformations observed by Rampal et al. (2008), for example, have a characteristic spatial scale of $\sim$10km, which is comparable to the eddy spatial scale and their imprint on sea ice, through the mechanisms occurring at the time of sea ice formation described for the first time here. Thus, understanding the interactions between oceanic eddies and the sea ice heterogeneity is critical to better understanding variations of the Arctic sea ice conditions and their evolution.

The Arctic sea ice cover has declined dramatically since the 1990s due to the rapid warming of the Arctic, as a consequence of anthropogenic forcing (Intergovernmental Panel on Climate Change (IPCC), 2022). As ice cover is declining, the Arctic is transitioning towards a seasonally ice-free regime (Crawford et al., 2021). Under this new paradigm, the ocean will experience a change in mechanical energy input and lateral temperature and salinity gradients at the ocean surface during ice-free seasons, resulting in an intensification of the ocean mesoscale and submesoscale fields (Li et al., 2024; Martin et al., 2014; McPhee, 2013). Our analyses suggest that an increase in the intensity of the eddy field results in a larger spatial variability in sea ice thickness over the freezing season. Therefore, characterizing the impacts eddies have in the sea ice thickness heterogeneity is crucial to better represent the interactions between the ice and the ocean and likely to better understand the transition towards a more energetic summer ice-free Arctic. The current generation of climate models lacks the resolution to represent eddy-sea ice interactions in the Arctic, therefore, including these interactions could reduce the uncertainties associated with the prediction of climate change in the Arctic.

Finally, our results show the importance of resolving the eddy field underneath forming sea ice. While the atmosphere is thought to be the main source of sea ice heterogeneity, here we show that eddies also play a role in setting up this heterogeneity. This eddy-driven heterogeneity is expected to occur in conjunction with other sources of heterogeneity, such as heterogeneity in the atmosphere, radiative fluxes, surface waves, and sea ice advection by winds. Thus, the relative importance of the eddy-induced heterogeneity discussed in this paper, and the feedback with other processes should be further explored. Missing processes such as winds and spatially varying radiative fluxes could generate instabilities and thus imprint further heterogeneity on sea ice (Gupta & Thompson, 2022). Our results focus on the Arctic Ocean, however, eddies in the Southern Ocean stand to impact the heterogeneity of the Antarctic sea ice through the same processes. Further research is required to describe and quantify the impact of eddies in high-resolution climate simulations, in addition to the joint impacts and contributions of eddies and winds in the heterogeneity of the Arctic sea ice and their preconditioning in the sea ice deformation.

7 Open Research

The idealized model configuration, the surface temperature, surface salinity, and fluxes of the model are described and publicly available at `https://github.com/josuemtzmo/Ice_formation` and `https://doi.org/10.5281/zenodo.10205736` respectively. All analyses and figures in this manuscript are reproducible via Jupyter notebooks and instructions can be found in the GitHub repository `Ice_formation` (`https://github.com/josuemtzmo/Ice_formation`).

Acknowledgments

We thank Till Wagner and an anonymous reviewer for their constructive feedback. We thank Clement Rousset and Martin Vancoppenolle for their invaluable help in creating the model set-up. We thank Anne-Marie Treguier and Angelina Cassianides for the constructive discussions that motivated some of the discussions described in the manuscript. We acknowledge funding from the ANR ImMEDIAT project (ANR-18-CE01-0010) and the MEDLEY project funded by the program JPI Ocean/JPI Climate (ANR-19-JPOC-0001) project. The idealized simulations and their analysis were performed using the HPC facilities DATARMOR of 'Pôle de Calcul Intensif pour la Mer' at Ifremer, Brest, France. We also acknowledge PRACE for awarding us access to Joliot-Curie at GENCI@CEA, France, where the SEDNA simulation has been performed.

References

Appen, W., Wekerle, C., Hehemann, L., Schourup-Kristensen, V., Konrad, C., & Iversen, M. H. (2018). Observations of a Submesoscale Cyclonic Filament in the Marginal Ice Zone. *Geophysical Research Letters*, *45*(12), 6141–6149. doi: 10.1029/2018gl077897

Aue, L., Vihma, T., Uotila, P., & Rinke, A. (2022). New insights into cyclone impacts on sea ice in the atlantic sector of the arctic ocean in winter. *Geophysical Research Letters*, *49*(22), e2022GL100051. doi: https://doi.org/10.1029/2022GL100051

Bashmachnikov, I. L., Raj, R. P., Golubkin, P., & Kozlov, I. E. (2023). Heat Transport by Mesoscale Eddies in the Norwegian and Greenland Seas. *Journal of Geophysical Research: Oceans*, *128*(2). doi: 10.1029/2022jc018987

Blanke, B., & Delécluse, P. (1993, July). Variability of the Tropical Atlantic Ocean Simulated by a General Circulation Model with Two Different Mixed-Layer Physics. *Journal of Physical Oceanography*, *23*, 1363–1388. doi: 10.1175/1520-0485(1993)023⟨1363:VOTTAO⟩2.0.CO;2

Brenner, S., Rainville, L., Thomson, J., & Lee, C. (2020). The evolution of a shallow front in the Arctic marginal ice zone. *Elem Sci Anth*, *8*, 17. doi: 10.1525/elementa.413

Carmack, E. C. (2007). The alpha/beta ocean distinction: A perspective on freshwater fluxes, convection, nutrients and productivity in high-latitude seas. *Deep Sea Research Part II: Topical Studies in Oceanography*, *54*(23-26), 2578–2598. doi: 10.1016/j.dsr2.2007.08.018

Cassianides, A., Lique, C., & Korosov, A. (2021). Ocean Eddy Signature on SAR-Derived Sea Ice Drift and Vorticity. *Geophysical Research Letters*, *48*(6). doi: 10.1029/2020gl092066

Cassianides, A., Lique, C., Tréguier, A., Meneghello, G., & Marez, C. (2023). Observed Spatio-Temporal Variability of the Eddy-Sea Ice Interactions in the Arctic Basin. *Journal of Geophysical Research: Oceans*, *128*(6). doi: 10.1029/2022jc019469

Crawford, A., Stroeve, J., Smith, A., & Jahn, A. (2021). Arctic open-water periods are projected to lengthen dramatically by 2100. *Communications Earth & Environment*, *2*(1), 109. doi: 10.1038/s43247-021-00183-x

Fine, E. C., MacKinnon, J. A., Alford, M. H., & Mickett, J. B. (2018). Microstructure observations of turbulent heat fluxes in a warm-core Canada Basin eddy Microstructure observations of turbulent heat fluxes in a warm-core Canada Basin eddy. *Journal of Physical Oceanography*, *48*(10), 2397–2418. doi: 10.1175/jpo-d-18-0028.1

Gupta, M., Marshall, J., Song, H., Campin, J., & Meneghello, G. (2020). Sea-Ice Melt Driven by Ice-Ocean Stresses on the Mesoscale. *Journal of Geophysical Research: Oceans*, *125*(11). doi: 10.1029/2020jc016404

Gupta, M., & Thompson, A. F. (2022). Regimes of Sea-Ice Floe Melt: Ice-Ocean Coupling at the Submesoscales. *Journal of Geophysical Research: Oceans*, *127*(9). doi: 10.1029/2022jc018894

Halloran, P. R., Hall, I. R., Menary, M., Reynolds, D. J., Scourse, J. D., Screen, J. A., ... Garry, F. (2020). Natural drivers of multidecadal Arctic sea ice variability over the last millennium. *Scientific Reports*, *10*(1), 688. doi: 10.1038/s41598-020-57472-2

Hersbach, H., Bell, B., Berrisford, P., Hirahara, S., Horányi, A., Muñoz-Sabater, J., ... Thépaut, J.-N. (2020). The era5 global reanalysis. *Quarterly Journal of the Royal Meteorological Society*, *146*(730), 1999-2049. doi: https://doi.org/10.1002/qj.3803

Horvat, C., & Tziperman, E. (2018). Understanding Melting due to Ocean Eddy Heat Fluxes at the Edge of Sea-Ice Floes. *Geophysical Research Letters*, *45*(18), 9721–9730. doi: 10.1029/2018gl079363

Intergovernmental Panel on Climate Change (IPCC). (2022). Polar regions. In *The ocean and cryosphere in a changing climate: Special report of the intergovernmental panel on climate change* (p. 203–320). Cambridge University Press. doi: 10.1017/9781009157964.005

Johannessen, O. M., Johannessen, J. A., Svendsen, E., Shuchman, R. A., Campbell, W. J., & Josberger, E. (1987). Ice-edge eddies in the fram strait marginal ice zone. *Science*, *236*(4800), 427-429. doi: 10.1126/science.236.4800.427

Kozlov, I. E., Plotnikov, E. V., & Manucharyan, G. E. (2020). Brief communication: Mesoscale and submesoscale dynamics in the marginal ice zone from sequential synthetic aperture radar observations. *The Cryosphere*, *14*(9), 2941–2947. doi: 10.5194/tc-14-2941-2020

Large, W., & Yeager, S. (2009). The global climatology of an interannually varying air–sea flux data set. *Climate Dynamics*, *33*(2-3), 341–364. doi: 10.1007/s00382-008-0441-3

Lewis, J. K., & Richter-Menge, J. A. (1998). Motion-induced stresses in pack ice. *Journal of Geophysical Research: Oceans*, *103*(C10), 21831–21843. doi: 10.1029/98jc01262

Li, X., Wang, Q., Danilov, S., Koldunov, N., Liu, C., Müller, V., ... Jung, T. (2024). Eddy activity in the Arctic Ocean projected to surge in a warming world. *Nature Climate Change*, 1–7. doi: 10.1038/s41558-023-01908-w

Locarnini, R., Mishonov, A., Antonov, J., Boyer, T., Garcia, H., Baranova, O., ... Johnson, D. (2010, 01). World ocean atlas 2009, vol. 1: Temperature. In S. Levitus (Ed.), (Vol. 68, p. 184).

Lu, K., Weingartner, T., Danielson, S., Winsor, P., Dobbins, E., Martini, K., & Statscewich, H. (2015). Lateral mixing across ice meltwater fronts of the Chukchi Sea shelf. *Geophysical Research Letters*, *42*(16), 6754–6761. doi: 10.1002/2015gl064967

Madec, G., Bourdallé-Badie, R., Chanut, J., Clementi, E., Coward, A., Ethé, C., ... Moulin, A. (2022, March). *Nemo ocean engine.* Zenodo. doi: 10.5281/zenodo.6334656

Manley, T. O., & Hunkins, K. (1985). Mesoscale eddies of the Arctic Ocean. *Journal of Geophysical Research: Oceans*, *90*(C3), 4911–4930. doi: 10.1029/jc090ic03p04911

Manucharyan, G. E., & Thompson, A. F. (2017). Submesoscale Sea Ice-Ocean Interactions in Marginal Ice Zones. *Journal of Geophysical Research: Oceans*, *122*(12), 9455–9475. doi: 10.1002/2017jc012895

Manucharyan, G. E., & Thompson, A. F. (2022). Heavy footprints of upper-ocean eddies on weakened Arctic sea ice in marginal ice zones. *Nature Communications*, *13*(1), 2147. doi: 10.1038/s41467-022-29663-0

Martin, T., Steele, M., & Zhang, J. (2014). Seasonality and long-term trend of

Arctic Ocean surface stress in a model. *Journal of Geophysical Research: Oceans*, *119*(3), 1723–1738. doi: 10.1002/2013jc009425

Mcnutt, S. L., & Overland, J. E. (2003). Spatial hierarchy in Arctic sea ice dynamics. *Tellus A*, *55*(2), 181–191. doi: 10.1034/j.1600-0870.2003.00012.x

McPhee, M. G. (2013). Intensification of Geostrophic Currents in the Canada Basin, Arctic Ocean. *Journal of Climate*, *26*(10), 3130–3138. doi: 10.1175/jcli-d-12-00289.1

Montgomery, R. B. (1940). The present evidence on the importance of lateral mixing processes in the ocean. *Bulletin of the American Meteorological Society*, *21*(3), 87–94.

Morison, J., Steele, M., Kikuchi, T., Falkner, K., & Smethie, W. (2006). Relaxation of central Arctic Ocean hydrography to pre-1990s climatology. *Geophysical Research Letters*, *33*(17). doi: 10.1029/2006gl026826

NEMO Sea Ice Working Group. (2022, March). *Sea ice modelling integrated initiative (SI^3) – the nemo sea ice engine* (No. 31). Zenodo. doi: 10.5281/zenodo.1471689

Nurser, A. J. G., & Bacon, S. (2014). The Rossby radius in the Arctic Ocean. *Ocean Science*, *10*(6), 967–975. doi: 10.5194/os-10-967-2014

Rampal, P., Weiss, J., Marsan, D., Lindsay, R., & Stern, H. (2008). Scaling properties of sea ice deformation from buoy dispersion analysis. *Journal of Geophysical Research: Oceans*, *113*(C3). doi: https://doi.org/10.1029/2007JC004143

Talandier, C., & Lique, C. (2023, February). *SEDNA-DELTA*. Zenodo. Retrieved from `https://doi.org/10.5281/zenodo.7656924` doi: 10.5281/zenodo.7656924

Webster, M. A., Rigor, I., & Wright, N. C. (2022). Observing arctic sea ice. *Oceanography*, *35*(3/4), pp. 29–37. doi: 10.5670/oceanog.2022.115

Figure 1.

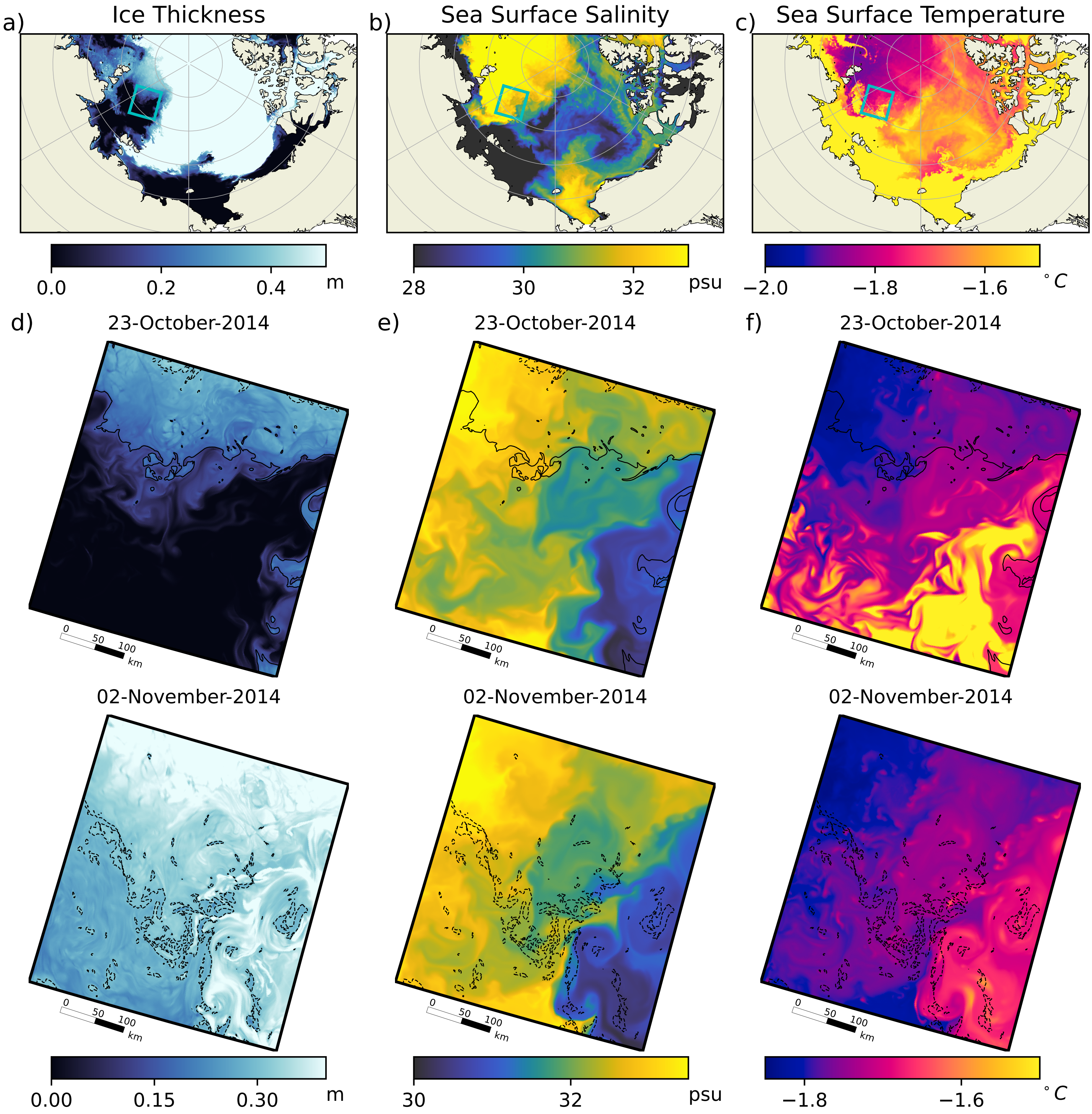
a)
Ice Thickness
b)
Sea Surface Salinity
c)
Sea Surface Temperature
0.0
0.2
0.4
m
28
30
32
psu
−2.0
−1.8
−1.6
°C
d)
23-October-2014
e)
23-October-2014
f)
23-October-2014
0
50
100
km
02-November-2014
02-November-2014
02-November-2014
0.00
0.15
0.30
m
30
32
psu
−1.8
−1.6
°C

Figure 2.

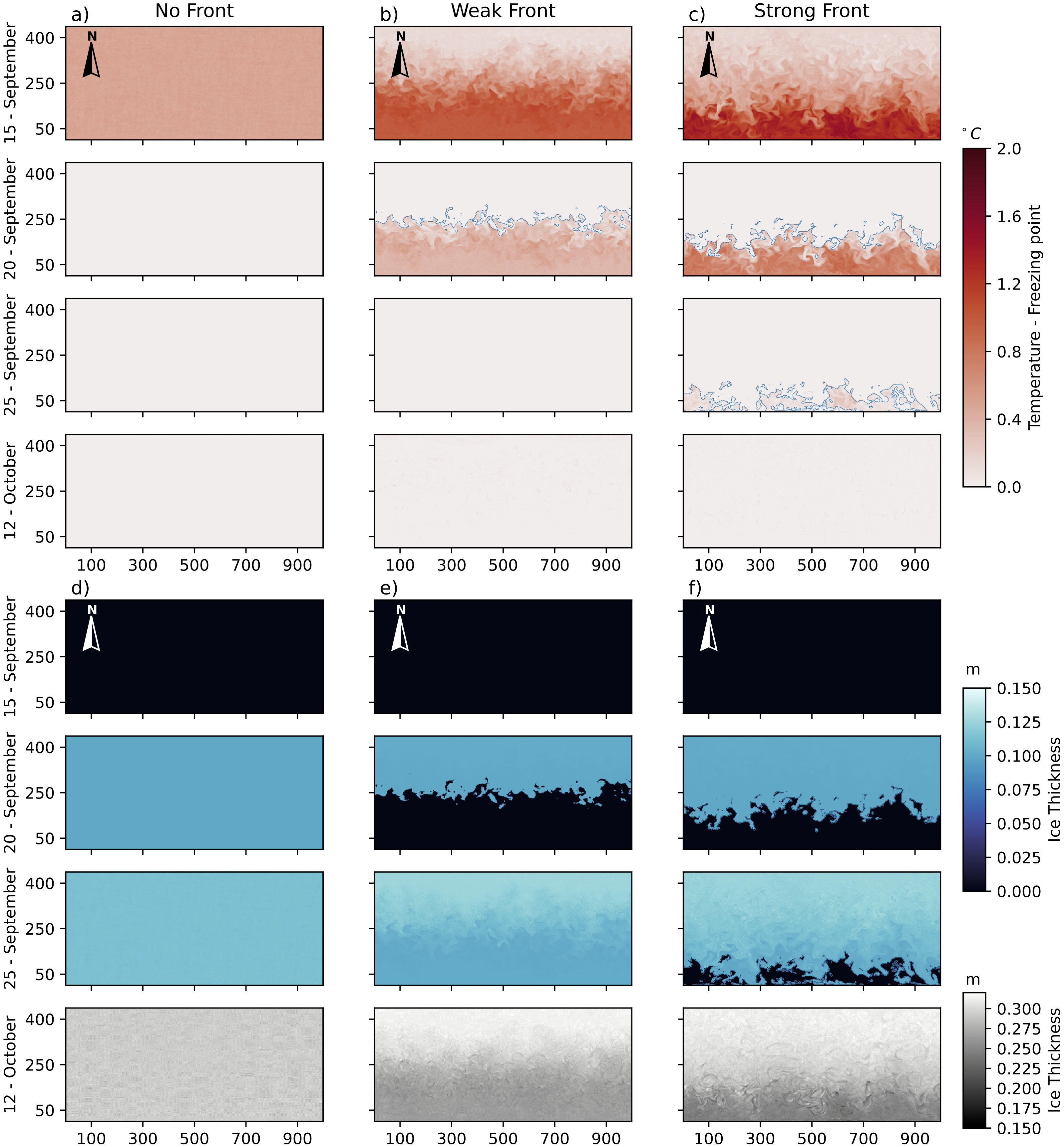

a) No Front
b) Weak Front
c) Strong Front
d)
e)
f)
N
15 - September
20 - September
25 - September
12 - October
400
250
50
100
300
500
700
900
°C
Temperature - Freezing point
2.0
1.6
1.2
0.8
0.4
0.0
m
Ice Thickness
0.150
0.125
0.100
0.075
0.050
0.025
0.000
m
Ice Thickness
0.300
0.275
0.250
0.225
0.200
0.175
0.150

Figure 3.

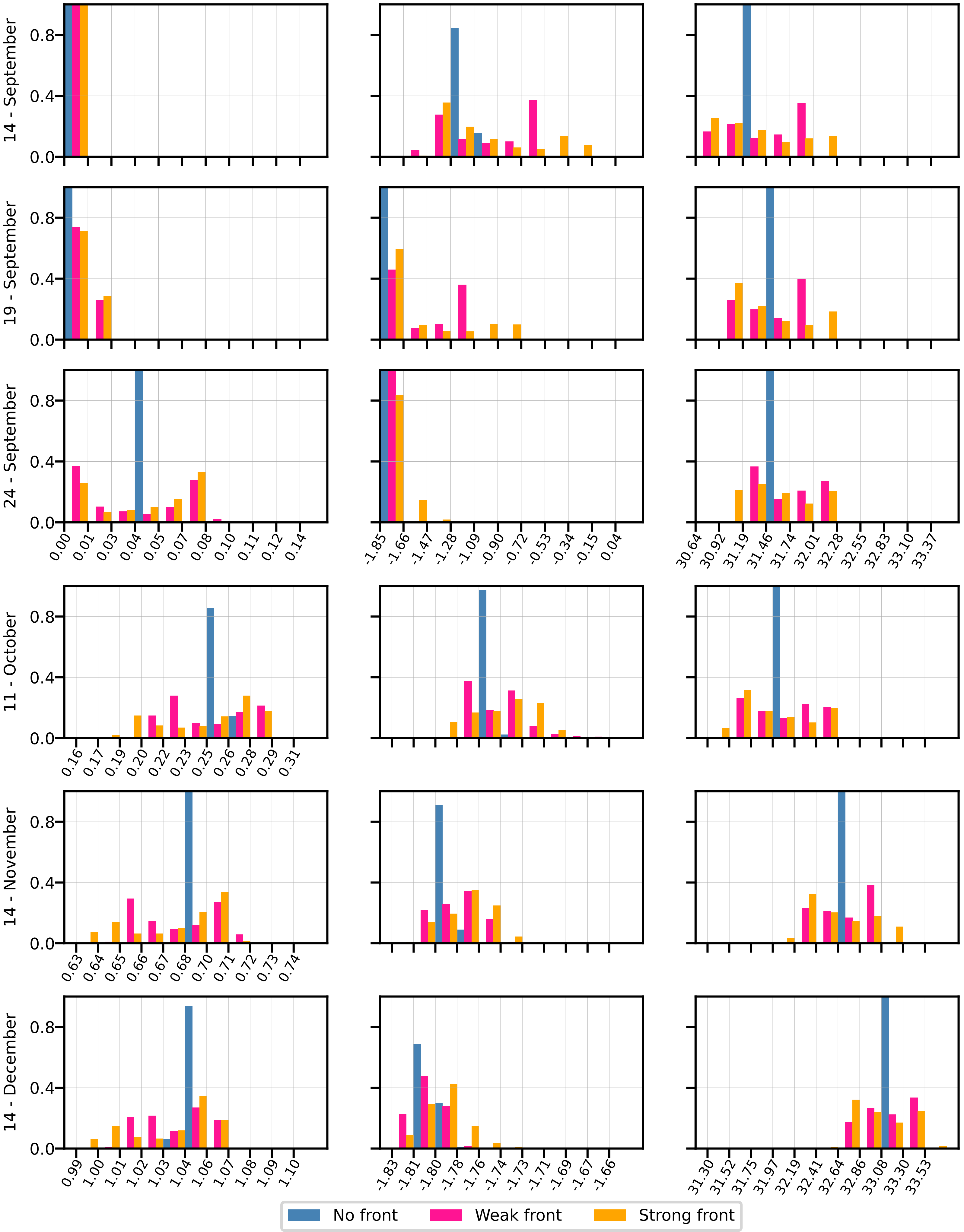
14 - September
19 - September
24 - September
11 - October
14 - November
14 - December
0.0
0.4
0.8
0.00 0.01 0.03 0.04 0.05 0.07 0.08 0.10 0.11 0.12 0.14
-1.85 -1.66 -1.47 -1.28 -1.09 -0.90 -0.72 -0.53 -0.34 -0.15 0.04
30.64 30.92 31.19 31.46 31.74 32.01 32.28 32.55 32.83 33.10 33.37
0.16 0.17 0.19 0.20 0.22 0.23 0.25 0.26 0.28 0.29 0.31
0.63 0.64 0.65 0.66 0.67 0.68 0.70 0.71 0.72 0.73 0.74
0.99 1.00 1.01 1.02 1.03 1.04 1.06 1.07 1.08 1.09 1.10
-1.83 -1.81 -1.80 -1.78 -1.76 -1.74 -1.73 -1.71 -1.69 -1.67 -1.66
31.30 31.52 31.75 31.97 32.19 32.41 32.64 32.86 33.08 33.30 33.53
No front
Weak front
Strong front

Figure 4.

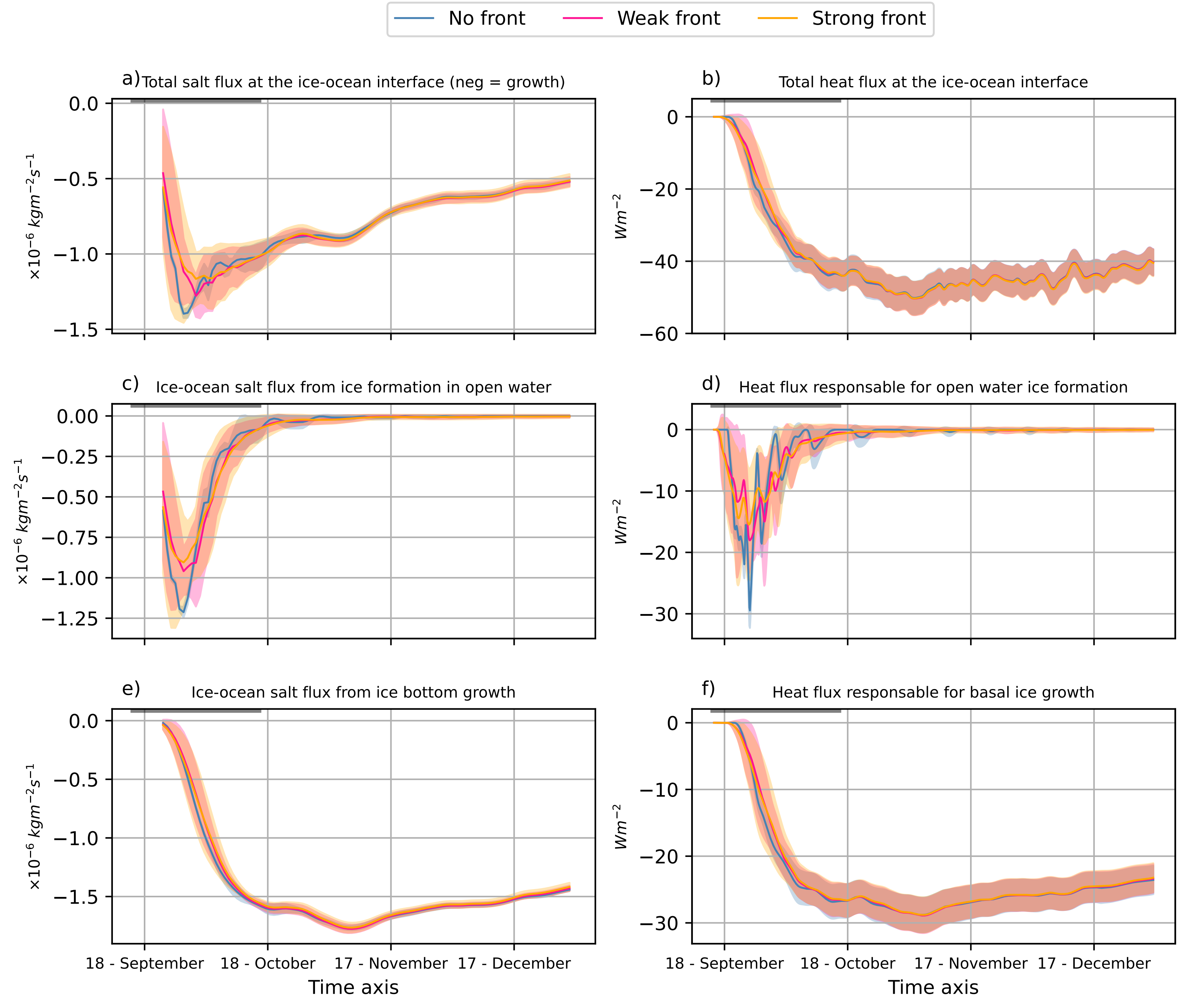
No front
Weak front
Strong front
a) Total salt flux at the ice-ocean interface (neg = growth)
b) Total heat flux at the ice-ocean interface
c) Ice-ocean salt flux from ice formation in open water
d) Heat flux responsable for open water ice formation
e) Ice-ocean salt flux from ice bottom growth
f) Heat flux responsable for basal ice growth
$\times10^{-6}\ kgm^{-2}s^{-1}$
Wm^{-2}
18 - September
18 - October
17 - November
17 - December
Time axis